Applied Materials Today 20 (2020) 100671

Contents lists available at ScienceDirect

Applied Materials Today

journal homepage: www.elsevier.com/locate/apmt

Mechanical metamaterials for full-band mechanical wave shielding

Lingling Wu[a,b,e,1], Yong Wang[c,1], Zirui Zhai[b], Yi Yang[a], Deepakshyam Krishnaraju[b], Junqiang Lu[d], Fugen Wu[e], Qianxuan Wang[a,*], Hanqing Jiang[b,*]

[a] College of Railway Engineering, Wuyi University, Jiangmen 529020, China
[b] School for Engineering of Matter, Transport and Energy, Arizona State University, Tempe AZ 85287, USA
[c] Department of Engineering Mechanics, Zhejiang University, Hangzhou 310027, Zhejiang, China
[d] Department of Physics, Zhejiang Normal University, Jinhua 321004, Zhejiang, China
[e] School of Materials and Energy, Guangdong University of Technology, 510006, China

ARTICLE INFO

Article history:
Received 25 February 2020
Revised 8 April 2020
Accepted 16 April 2020

Keywords:
Mechanical metamaterial
Energy circulation
Vibration isolation
Shield
Full band

ABSTRACT

The manipulation of the interactions between matter and waves is the central theme of metamaterials. The capability of energy shielding in a full frequency band has not yet been achieved. In this paper, a mechanical metamaterial for perfect energy shielding was discovered through a new mechanism by solely circulating energy between a metamaterial and an energy source. Unprecedented energy shielding effects are experimentally demonstrated in low and ultralow vibrational frequency ranges. Along with the widely explored mechanisms, namely, the "energy bypass" and "energy absorption" mechanisms, the "energy shield" mechanism and demonstrated mechanical metamaterial in this paper open a new direction for the design of metamaterials with unprecedented dynamic characteristics in various physical systems at different length scales.

1. Introduction

The control or manipulation of the flow of mechanical energy in terms of waves or vibrations holds a pivoting position for the discovery of mechanical metamaterials [1–3]. As mechanical energy is applied to a composite consisting of an encased object (i.e., a payload) and surrounding metamaterials, one or both of the work conjugate variables (e.g., force and displacement) must inevitably be applied to the composite. The design of mechanical metamaterials aims to control the interactions between the input mechanical energy and the metamaterial, which can be achieved in two ways, namely, energy bypassing and energy localization. As the name suggests, energy bypassing deviates the input energy from the payload by employing a set of materials with spatially dependent material properties, such as stiffness and density; energy localization confines the input energy inside the metamaterial through a local resonance. Consequently, the payload does not "feel" the existence of the input mechanical energy in both cases. These two methods have been applied to experimentally achieve fascinating performance, including acoustic cloaking [4] and acoustic metamaterials [5], although the methods still have inevitable limitations. Energy bypassing requires materials to be rigorously distributed in space following preciously defined mathematical expressions, which cannot be achieved by state-of-the-art manufacturing; thus, the experimental performance is not as ideal as the theoretical prediction. Energy localization using a local resonance usually performs well in a limited frequency regime and at a specific frequency. In a practical application, the localized energy is easily transferred into other forms, such as heat or electromagnetic radiation, which might have a band effect on the surrounding environment.

Recent advances in micro- and nanofabrication [6], topological optimization [7], machine learning [8], and three-dimensional (3D) printing [9] are transforming gadgets from science fiction into realistic artificial materials, i.e., metamaterials [10–12]. Examples include electromagnetic (EM) cloak enabled by metamaterials that control the interactions between EM waves and matter [13–17], and demonstrations have achieved a perfect lens [18], an absorber [19], and cloaking [20]. Exotic properties [3,21–26], such as auxetics [7,27–28], negative thermal expansion [26,29], multistability [30–31], and elastomechanical cloaking [32], have been achieved by mechanical metamaterials. Acoustic metamaterials, a subset of mechanical metamaterials initially created for use in sound-attenuation applications, focus on the control of acoustic waves over a specific bandwidth. Today, achieving complete attenuation of acoustic energy over a full frequency band, i.e., perfect acoustic energy shielding to block environment noise, is still one of the ultimate goals of acoustic metamaterials [33]. An energy shield

* Corresponding authors.
E-mail addresses: wydxwqx@wyu.edu.cn (Q. Wang), hanqing.jiang@asu.edu (H. Jiang).
[1] These authors contributed equally to this paper

https://doi.org/10.1016/j.apmt.2020.100671
2352-9407/

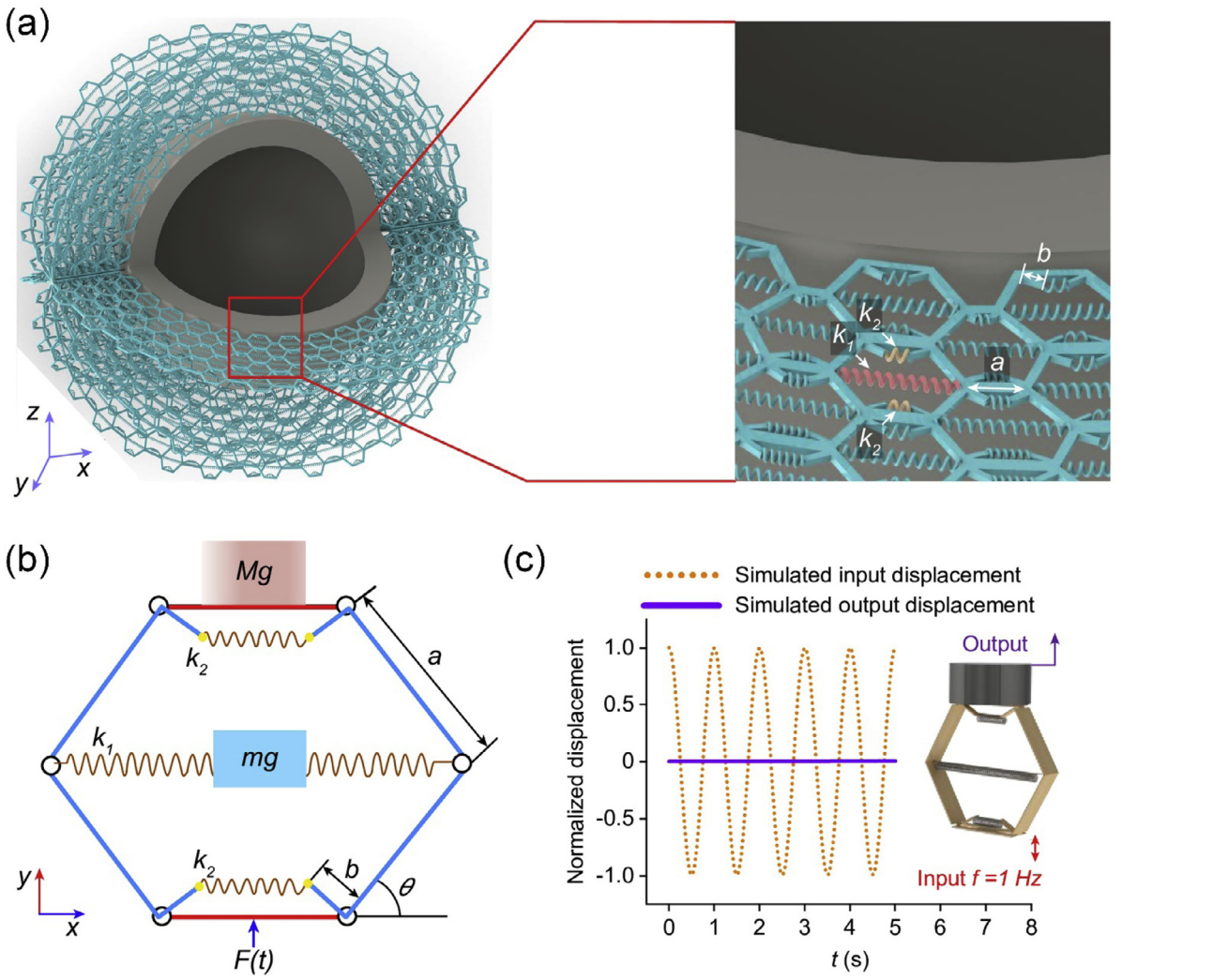

Fig. 1. (a) Illustration of the mechanical metamaterials as a shell to shield the object in the core (i.e., payload) from the input energy flux. (b) An arbitrary state of the mechanical metamaterial given by the angle θ. (c) Performance of the proposed vibration isolator at 1 Hz using finite element simulations.

encases and protects an object from the input energy flux but has not been realized by various mechanical metamaterials.

The requirement of a perfect energy shield is to completely isolate the payload from the input energy. In other words, the state of the payload (e.g., equilibrium for a mechanical system) should not be altered by the input energy flux; thus, the payload does not "feel" the input energy flux. In this paper, we present a unit cell of a mechanical metamaterial (i.e., meta-atom) that can circulate the energy between the metamaterial and an energy source and thus exert a constant force on the payload. The input energy-independent constant force suggests that the state of the payload is independent of the input energy flux, which can find numerous applications, such as vibration isolation. This paper shows that the present mechanical metamaterial is indeed a metamaterial with absolute-zero-stiffness, which isolates vibrations in low and ultralow frequency ranges (e.g., lower than 20 Hz) that are harmful to our health because of the resonance of human organs [34–37]. The basic principle of designing a perfect energy shield, i.e., solely circulating the input energy between the energy source and the metamaterials, represents a new mechanism to design mechanical metamaterials for the manipulation of wave propagation and can find applications in various areas of physics, such as the control of acoustic waves at mm–cm scales and thermal insulation at atomistic scales.

2. Theory

Fig. 1(a) illustrates a composite structure with mechanical metamaterials as a shell to shield the input energy flux from the payload in the core. Before the input energy is applied to the composite, the payload is subjected to forces and/or moments (e.g., gravitational force or forces exerted from the surrounding metamaterials) and is in an equilibrium state. Upon energy flux, the mechanical metamaterial shell will further deform and only allow the energy to circulate between the shell and the energy source. The forces exerted on the payload remain unchanged. The unit cell of the mechanical metamaterial consists of springs and inextensible bars.

The analysis of a unit cell carrying a dead load (e.g., a mass block with weight Mg) shown in Fig. 1(b) explains why this metamaterial isolates the input energy from the payload (i.e., the mass block). Before the input energy is applied to the metamaterial, the payload is in an equilibrium state; i.e., the force exerted from the metamaterial to the payload balances the weight Mg. To isolate the input energy or vibration from the environment $F(t)$, the states of the payload, e.g., equilibrium and position, must not change; thus, the force exerted from the metamaterial to the payload remains Mg. To obtain the necessary conditions for vibration energy isolation over a full frequency band, quasistatic ($f \approx 0$ Hz) anal-

ysis is employed to explore the relationships among the parameters, i.e., the geometrical parameters a and b, spring constants k_1 and k_2, mass of the metamaterial m, and state of the metamaterial unit θ, with $\theta = 0$ for a completely collapsed state and $\theta = 90^\circ$ for a completely deployed state. Under static equilibrium, $F(t) = F_0 = (M+m)g$. To ensure that the state of the payload remains unchanged at any value of θ, the input energy $W_{input} = 2a(M+m)(1-\sin\theta)g$ must be completely converted to the potential energy of the metamaterials, including the spring energy and the gravitational potential energy of the metamaterial, i.e., $W_{potential} = mga(1-\sin\theta) + 4b^2k_2(1-\sin\theta)^2 + 2a^2k_1\cos^2\theta$. Equating W_{input} and $W_{potential}$, one can obtain the following relations: $(1): \frac{k_1}{k_2} = 2(\frac{b}{a})^2$, and $(2): k_1 = \frac{(2M+m)g}{4a}$. These two requirements ensure that the payload can reach equilibrium at any given location described by θ. In other words, the metamaterial has zero effective stiffness (see Fig. S1 of Supporting Information) and isolates the input energy from the payload. Static force analysis in Fig. S2 of Supporting Information also verifies that a constant force is exerted from the metamaterial to the payload and a constant zero stiffness is achieved during the entire displacement range. As long as the two equations are satisfied, the input energy $\boldsymbol{W}_{input}$ will always equals to the potential energy $\boldsymbol{W}_{potential}$ stored in the springs. When θ decreases, energy will be stored in the system and when θ increases, the energy stored in the model will be released to the surroundings, which we call an "energy circulation."

Next, we show that under these two requirements, the metamaterial can isolate the payload from the environment under arbitrary dynamic loads. Dynamic analysis is performed using Lagrangian mechanics: $\frac{d}{dt}(\frac{\partial L}{\partial \dot{q}_j}) - \frac{\partial L}{\partial q_j} = Q_{q_j}$. Here, $\{q_1, q_2\} = \{y, \theta\}$ are generalized displacements; $\{\dot{q}_1, \dot{q}_2\} = \{\dot{y}, \dot{\theta}\}$ are generalized velocities; $\{Q_{q_1}, Q_{q_2}\} = \{F(t), 0\}$ are generalized forces; and $L = T - U$ is the Lagrangian with T and U being the kinetic and potential energies, respectively. As detailed in the Supporting Information, we have shown that a constant force Mg is exerted from the mechanical metamaterial to the payload when a dynamic input force $F(t)$ is applied to the mechanical metamaterial; consequently, the payload remains static under dynamic loading of the metamaterial – the metamaterial perfectly shields the payload from the environment vibration and operates over the full band. Fig. 1(c) shows a finite element result where a sinusoidal input displacement with a frequency of 1 Hz is applied to the bottom of the mechanical metamaterial. It is apparent that there is a vanishing displacement at the payload. Video S1 shows the video from this simulation.

The mechanism of this intriguing performance is that the input energy solely circulates between the metamaterial and the energy source and thus does not affect the payload. A natural question to ask is whether this mechanism can only lead to this particular structure in Fig. 1(b). To address this question, we utilize a genetic algorithm (GA) to perform the design under the constraint that the mechanical metamaterial has six sides in a hexagon shape. A model with arbitrary design parameters is constructed using commonly used components (i.e., mass block, truss, and springs), as shown in Fig. S4 of Supporting Information. The GA is executed in the Global Optimization Toolbox™ in MATLAB. The GA finds all possible combinations of the design variables to minimize the difference between the total input energy and the change in the potential energy of the metamaterial. As detailed in the Supporting Information, the GA searches among the design variables by repeatedly modifying a population of individual solutions to find a combination(s) to achieve perfect energy shielding using the mechanism identified in this paper. Fig. S5 of Supporting Information shows the process of the structural evolution with 6 steps, and each step evolves for 1,000 generations. In each step, we reach a

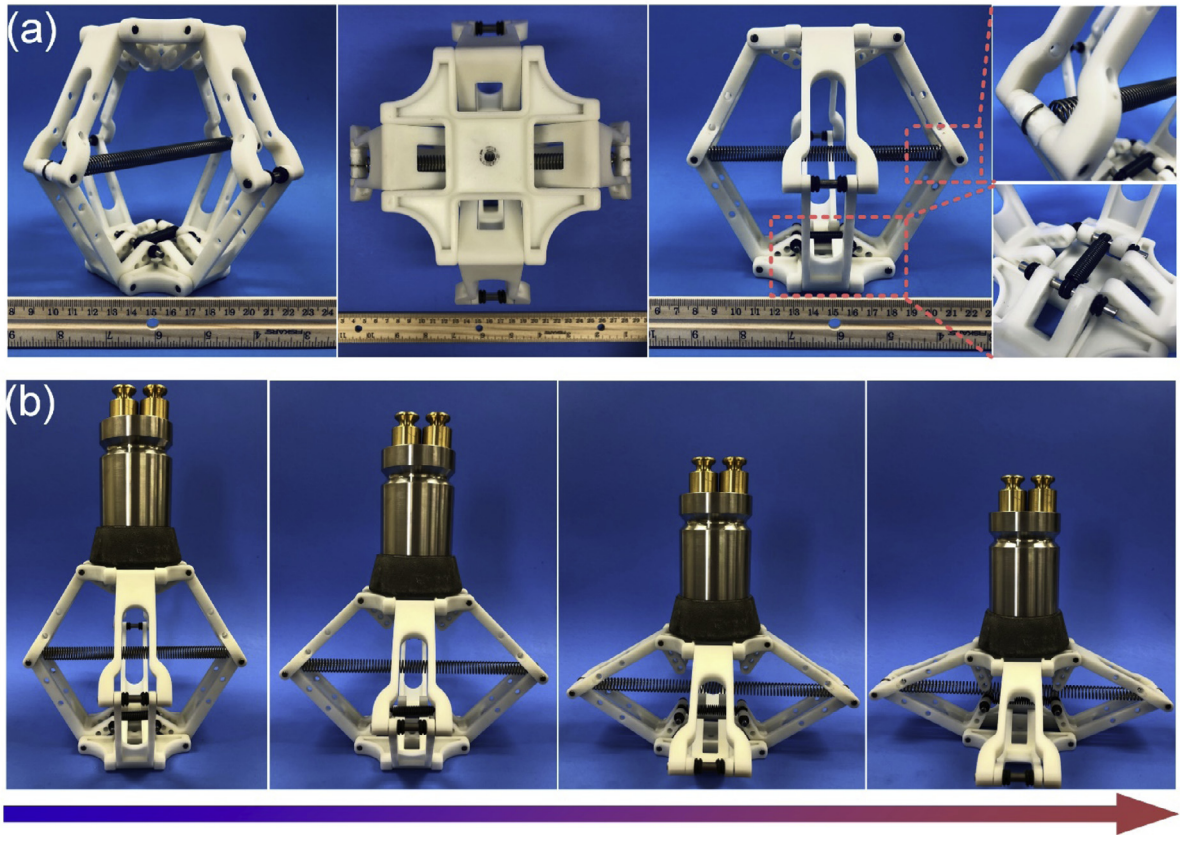

Fig. 2. (a) Photographs of the fabricated metamaterial. (b) Equilibrium of the metamaterial at any position.

partially optimal metamaterial with a narrow range of some parameters. For example, from step 1 after 1,000 generations, we fixed the location of the vertical spring in the metamaterial and started subsequent evolution steps. As shown in Fig. S5 of Supporting Information, the GA finds many metamaterial candidates (actually infinity if the simulation continues running) that can achieve perfect energy shielding. These metamaterials can be divided into three categories (Fig. S6 of Supporting Information). The first design that corresponds to the model given in Fig. 1(b) is chosen given practical engineering constraints, such as the lack of compression springs, fewer components, and the fabrication simplicity. A similar approach can be employed to create other metamaterials (not just mechanical metamaterials) based on a mechanism that solely circulates the energy between the metamaterial and the energy source.

3. Experimental section

3.1. Preparation of metamaterial sample

The metamaterial was fabricated by a 3D printing process. Curable resin was used as the component material to print the framework of the sample, and stainless-steel rods were adopted as hinges to join the elements together. Rubber stoppers were installed on each end of the rods to keep the hinge tight. The springs utilized here were from MiSUMi-VONA, with model numbers UFSP12-1.2-90 for the primary spring and WFSP9-1.2-30 for the secondary spring. The mass m of the metamaterial was neglected since it is much smaller than the mass M of the payload. Fig. 2(a) shows the mechanical metamaterial where only one of the shorter springs (k_2) is mounted to reduce the balanced weight by half with $\frac{k_1}{k_2} = (\frac{b}{a})^2$ and $Mg = 2ak_1$. Note that a symmetric configuration was adopted to prevent unintentional leaning due to manufacturing or vibration. The attribute of a constant force (shown in Fig. S1 of Supporting Information) was verified by achieving balance at any position when the matching weight ($Mg = 2ak_1$) was applied quasistatically, as suggested in Fig. 2(b).

3.2. Experiment setup

The vertical and horizontal experimental setups are shown in Fig. 3(a) and Fig. 3(e), respectively. In the vertical experiment, one metamaterial was installed on an electromechanical shaker (S 51120 from TIRA vibration Test Systems Inc.). The payload was appropriately adjusted by standard weights and was attached on the surface of the metamaterial. Two identical accelerators (352C33 from PCB Piezotronics Inc.) were attached on the top and bottom surfaces of the metamaterial, located at the excitation and output positions, respectively. In the horizontal experiment, the payload (a cart with wheels to reduce the influence of friction) was connected by two horizontal shakers: a right shaker (S 51120 from TIRA vibration Test Systems Inc.) and a left shaker (ET-139 from Labworks Inc.). Three accelerometers (two 352C33 accelerometers from PCB Piezotronics Inc. and one 356A25 accelerometer from PCB Piezotronics Inc.) were attached on the excitation positions and the payload. The random/sweep signal(s) were generated by the signal generation module included in the dynamic signal collection system (LabGenius IM1208H from Inter-Measure, Inc.), and then amplified by power amplifiers (BAA 120 from TIRA vibration Test Systems Inc. and pa-138 from Labworks Inc.). The acceleration signals were measured and directly acquired by the dynamic signal collection system.

3.3. Results and discussion

To test the performance of the metamaterial in shielding energy in the vertical directions, a random vibration with a power spectrum spreading in the frequency interval of [0, 25] Hz was generated by a shaker and applied to the bottom of the metamaterial. Comparisons of the output and input accelerations for a random vibration and a frequency sweep are shown in Fig. 3(b–c), respectively, which clearly demonstrate that the output acceleration measured at the payload is vanishingly small compared with the input acceleration. This result experimentally verifies the prominent vibration energy shielding effect. The transmissibility in dB defined by $20\log|\frac{a_{ouput}}{a_{input}}|$, where a_{output} is the acceleration at the payload and a_{input} is the acceleration generated by the shaker, for low and ultralow frequency ranges (Fig. 3(d)) shows that this mechanical metamaterial can significantly shield vibrations over almost the entire measured frequency band, from as low as 0.1–25 Hz. . The low frequency motion of the payload shown in Video S2 and S3 is caused by the fabrication error (*e.g.*, geometrical deviation), the friction between contact surfaces, and the measurement discrepancy (*e.g.*, the accelerators in the experiment are 352C33 from PCB Piezotronics Inc., which cannot accurately capture the accelerations when the frequency is lower than 0.1 Hz). Besides, in theory, the mass of the payload (M) should be much larger than that of the isolator itself (m). In our experiment, $M \approx 10$ m. Therefore, the performance in ultra-low frequency is not as good as higher frequency. Despite all of the experiment discrepancies, the model could still suppress the motion of payload in low-frequency range which could be illustrated by simply comparing the two eggs in Video S4. This mechanical metamaterial outperforms all reported quasizero-stiffness isolators [35,38–44] and many active vibration isolators [45–46]. Video S2 and S3 show the results for the random vibration and frequency sweep, respectively.

Fig. 3(e) shows the experimental setup used to test the performance of the metamaterial in shielding energy in the horizontal directions. Here, two identical metamaterials and a sandwiched payload were used. Two shakers individually impose random forces on the metamaterials. Here, the gravitational potential energy becomes irrelevant; thus, the static analysis given by Fig. S2 can show that a constant force $2ak_1$ is exerted from the metamaterial to the payload. The symmetry of the setup ensures that the sandwiched payload is always subjected to a pair of constant forces .. in opposite directions; thus, the state of the payload is independent of the applied forces. Lagrangian mechanics was employed to analyze the dynamic performance, and the analysis found that the sandwiched payload is stationary and does not depend on the input force(s) (see Fig. S7 of Supporting Information). Fig. 3(f) verifies that the output acceleration measured at the payload vanishes compared with the input accelerations of shakers 1 and 2. Fig. 3(g) shows that the metamaterials can still isolate vibrations when the vibration is only from shaker 1 while shaker 2 is inactive. The transmissibility for the low and ultralow frequency ranges (Fig. 3(h)) again shows that this mechanical metamaterial can significantly shield input random forces when only one shaker is active. Videos S5 and S6 show the results for a random vibration excited by only one shaker and two shakers in the horizontal directions, respectively.

As demonstrated previously by theoretical analysis, when the gravitational potential field enters the design, such as in Fig. 1, one requirement is $k_1 = \frac{(2M+m)g}{4a}$; equivalently, when the spring and geometry are chosen, the mass of the payload is determined and the constant force exerted by the mechanical metamaterial is fixed. Considering the practical application, we modified a model to achieve tunable payloads by using the same metamaterial characterized by the spring constants and geometry. Two new design parameters $\Delta a$and Δb were introduced to allow springs with ad-

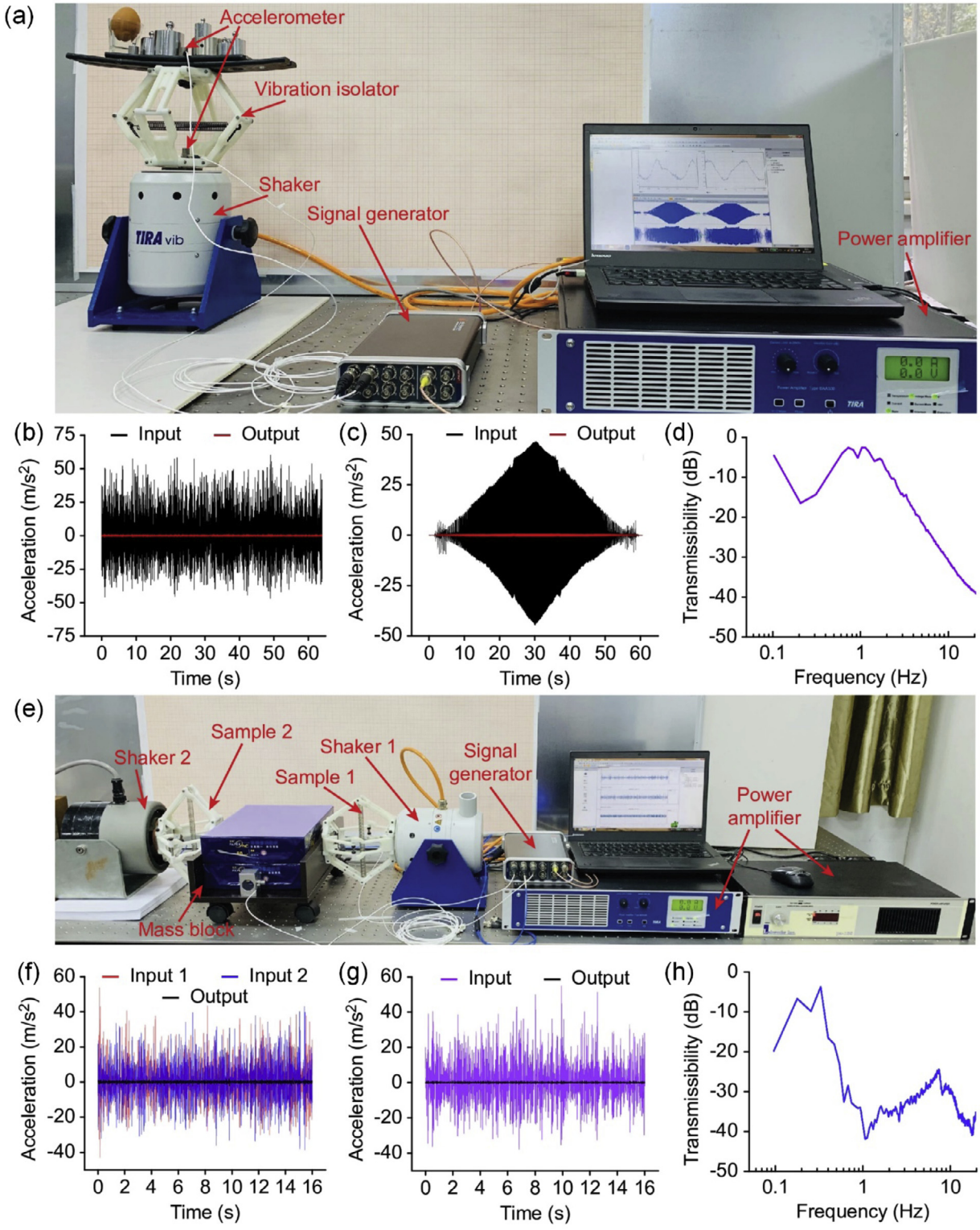

Fig. 3. Experimental setup and results. (a) Instrument setup to measure the vertical performance of the mechanical metamaterials. (b) Comparison of the measured input and output accelerations for a random vibration. (c) Comparison of the measured input and output accelerations for a frequency sweep excitation. (d) Measured frequency response curve for a vertical vibration. (e) Instrument setup to measure the horizontal performance of the metamaterials. (f) Comparison of the measured input and output accelerations when two shakers individually exert random forces on the payload. (g) Comparison of the measured input and output accelerations when only one (the right) shaker exerts a random force on the payload. (h) Measured frequency response curve.

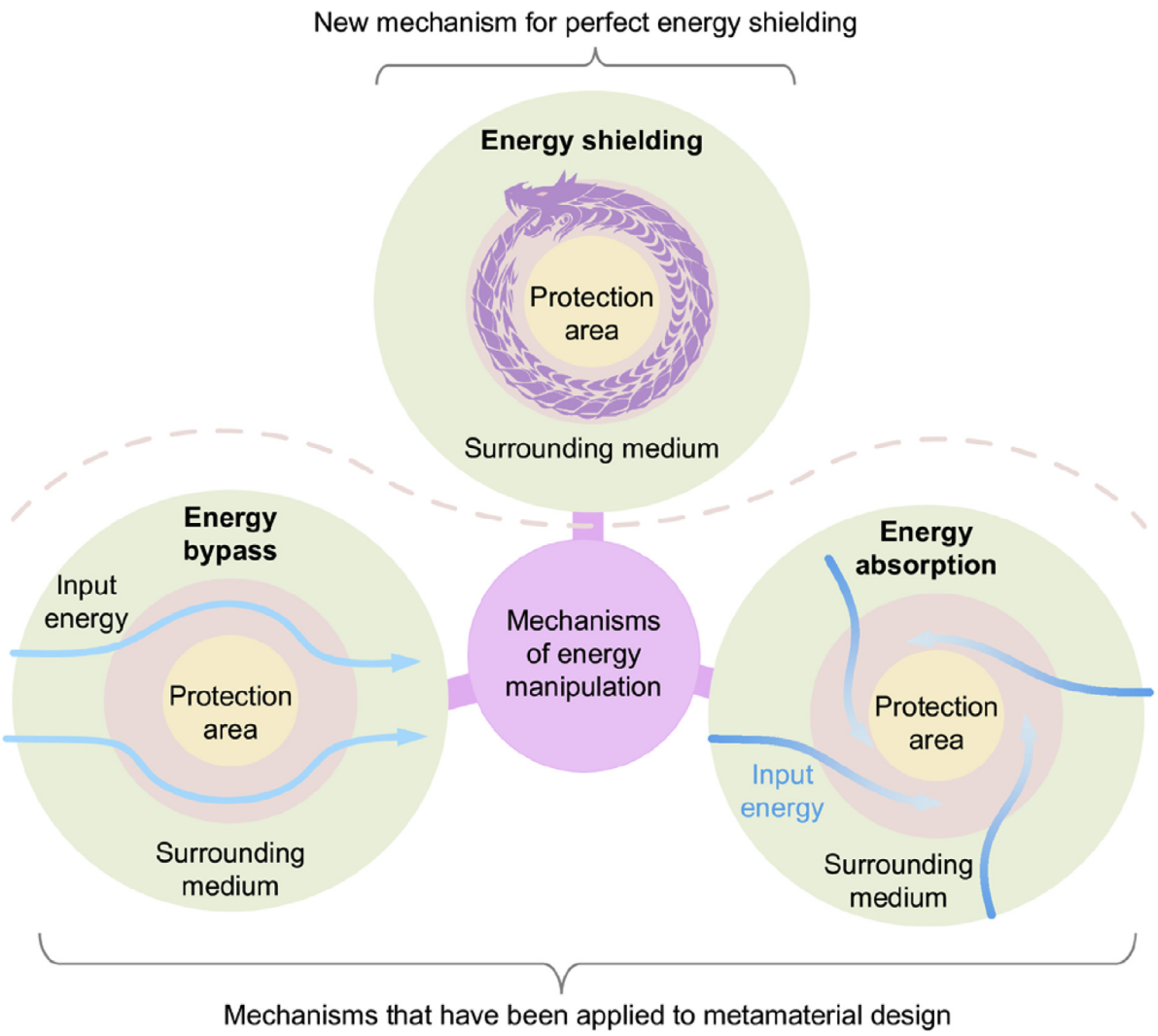

Fig. 4. Three mechanisms for energy protection.

justable positions. As shown in the Fig. S8 of Supporting Information, the mass of the payload can be adjusted while shielding the payload from the input energy.

A mechanical metamaterial with repeating units was also constructed. Simulations for both one-dimensional (Videos S7–S9) and two-dimensional directions cases (Video S10) were carried out to demonstrate the energy shielding performance of the metamaterial. As detailed in Fig. S9 of Supporting Information, the merits of metamaterial arrays include better energy isolation performance, higher tolerance for the uncertainties, and a higher load bear capability.

4. Conclusion

In summary, this paper discovers a new mechanical metamaterial as a perfect energy shield by utilizing an unexplored design mechanism: circulating the energy between the metamaterial and the energy source, without passing energy to the payload. The present mechanical metamaterial has absolute-zero-stiffness and thus can function as a vibration isolator for the full frequency band. Upon applying dynamic loads to the payload, the mechanical metamaterial exerts a constant force on the payload, with or without a gravitational potential field; thus, the state of the payload is perfectly shielded from the input energy. Unprecedented shielding effects are experimentally demonstrated in low and ultralow frequency ranges. Different from many active systems (e.g., the head/neck of birds has been noticed and studied for decades [47] because of its ability to maintain the stability of a bird's head through an active feedback system in the bird's body and has inspired the development of active systems consisting of sensors, actuators and processors to counteract the input energy for shielding), the present mechanical metamaterials are passive and provide ideal shielding for input vibration energy. This metamaterial also significantly advances the development of passive systems, such as quasizero-stiffness systems combining positive and negative stiffness components together to construct a nonlinear system with a quasizero effective stiffness in a small range (Fig. S10 of Supporting Information), because the present mechanical metamaterials are effective for a full frequency band while most of the quasizero-stiffness systems can only shield input energy in a narrow amplitude range and cannot be applied to low and ultralow frequency ranges.

Although the principle is demonstrated with a mechanical metamaterial for vibration isolation, it can also be applied to other physical fields. For example, as shown in Fig. S11 of Supporting Information, a similar electromechanical metamaterial was built by replacing the mass block in Fig. 1(b) with a capacitor that stores electrical energy. This electromechanical metamaterial might be used to isolate the vertical mechanical energy in a zero-gravity environment. In fact, the principle in this paper suggests a third

mechanism for energy protection. As shown in Fig. 4, the first two "energy bypass" and "energy absorption" mechanisms have been successfully explored to guide dynamic waves with applications such as electromagnetic wave cloaking (electric field) and sound wave stealth technology (acoustic field). The "energy shield" mechanism, presenting an Ouroboros-type feature, can be used for other physical systems at various length scales. For example, perfect thermal isolation may become feasible using the same principle, since zero-stiffness materials can insulate thermal conduction in solids. Overall, the principle presented in this paper opens a new direction for the design of metamaterials with unprecedented dynamic characteristics that can be employed to manipulate the interactions between matter and waves.

Data availability

The raw/processed data required to reproduce these findings cannot be shared at this time as the data also forms part of an ongoing study.

Declaration of Competing Interest

None.

CRediT authorship contribution statement

Lingling Wu: Conceptualization, Methodology, Software, Writing - original draft, Writing - review & editing. **Yong Wang:** Conceptualization, Methodology, Writing - review & editing. **Zirui Zhai:** Conceptualization. **Yi Yang:** Writing - review & editing. **Deepakshyam Krishnaraju:** Writing - review & editing. **Junqiang Lu:** Methodology. **Fugen Wu:** Methodology. **Qianxuan Wang:** Methodology, Software. **Hanqing Jiang:** Conceptualization, Methodology, Software, Writing - original draft, Writing - review & editing.

Acknowledgments

H. Jiang. acknowledges the support from the National Science Foundation under Grant No. CMMI-1762792. L. Wu acknowledges the Guangdong Young Talents Project under Grant No. 2018KQNCX269 and the Special Funds for the Cultivation of Guangdong College Students' Scientific and Technological Innovation under Grant No. pdjh2020b0598. Y. Wang acknowledges the National Natural Science Foundation of China under Grant Nos. 11872328, 11532011 and 11621062 and the Fundamental Research Funds for the Central Universities under Grant No. 2018FZA4025. Q. Wang acknowledges the National Key Research and Development Program of China: Thirteenth Five-Year Advanced Rail Transit Key Project under Grant No.2018YFB1201601. We would like to thank Dr. Yanchao Hu from ZP Test Inc. for technical support and helpful discussions. L. Wu and Y. Wang contributed equally to this work.

Supplementary materials

Supplementary material associated with this article can be found, in the online version, at doi:10.1016/j.apmt.2020.100671.

Appendix A. Supporting data

Supporting data to this article can be found online.

References

[1] T. Frenzel, J. Kopfler, E. Jung, M. Kadic, M. Wegener, Ultrasound experiments on acoustical activity in chiral mechanical metamaterials, Nat. Commun. 10 (1) (2019) 3384, doi:10.1038/s41467-019-11366-8.
[2] Z. Zhai, Y. Wang, H. Jiang, Origami-inspired, on-demand deployable and collapsible mechanical metamaterials with tunable stiffness, Proc. Natl. Acad. Sci. U. S. A. 115 (9) (2018) 2032–2037, doi:10.1073/pnas.1720171115.
[3] X. Yu, J. Zhou, H. Liang, Z. Jiang, L. Wu, Mechanical metamaterials associated with stiffness, rigidity and compressibility: a brief review, Prog. Mater. Sci. 94 (2018) 114–173, doi:10.1016/j.pmatsci.2017.12.003.
[4] S. Zhang, C. Xia, N. Fang, Broadband acoustic cloak for ultrasound waves, Phys. Rev. Lett. 106 (2) (2011) 024301, doi:10.1103/PhysRevLett.106.024301.
[5] X. Xu, M.V. Barnhart, X. Li, Y. Chen, G. Huang, Tailoring vibration suppression bands with hierarchical metamaterials containing local resonators, J. Sound Vib. 442 (2019) 237–248, doi:10.1016/j.jsv.2018.10.065.
[6] R. Garcia, A.W. Knoll, E. Riedo, Advanced scanning probe lithography, Nat. Nanotechnol. 9 (2014) 577–587, doi:10.1038/nnano.2014.157.
[7] A. Clausen, F. Wang, J.S. Jensen, O. Sigmund, J.A. Lewis, Topology optimized architectures with programmable poisson's ratio over large deformations, Adv. Mater. 27 (37) (2015) 5523–5527, doi:10.1002/adma.201502485.
[8] K.T. Butler, D.W. Davies, H. Cartwright, O. Isayev, A. Walsh, Machine learning for molecular and materials science, Nature 559 (7715) (2018) 547–555, doi:10.1038/s41586-018-0337-2.
[9] R.L. Truby, J.A. Lewis, Printing soft matter in three dimensions, Nature 540 (7633) (2016) 371–378, doi:10.1038/nature21003.
[10] J.B. Pendry, D. Schurig, D.R. Smith, Controlling electromagnetic fields, Science 312 (5781) (2006) 1780–1782, doi:10.1126/science.1125907.
[11] D.R. Smith, J.B. Pendry, M.C.K. Wiltshire, Metamaterials and negative refractive index, Science 305 (5685) (2004) 788–792, doi:10.1126/science.1096796.
[12] E. Barchiesi, M. Spagnuolo, L. Placidi, Mechanical metamaterials: a state of the art, Math. Mech. Solids 24 (1) (2018) 212–234, doi:10.1177/1081286517735695.
[13] D. Schurig, J.J. Mock, B.J. Justice, S.A. Cummer, J.B. Pendry, A.F. Starr, D.R. Smith, Metamaterial electromagnetic cloak at microwave frequencies, Science 314 (5801) (2006) 977–980, doi:10.1126/science.1133628.
[14] D. Shin, Y. Urzhumov, Y. Jung, G. Kang, S. Baek, M. Choi, H. Park, K. Kim, D.R. Smith, Broadband electromagnetic cloaking with smart metamaterials, Nat. Commun. 3 (2012) 1213, doi:10.1038/ncomms2219.
[15] E.A. Chan, S.A. Aljunid, G. Adamo, A. Laliotis, M. Ducloy, D. Wilkowski, Tailoring optical metamaterials to tune the atom-surface Casimir-Polder interaction, Sci. Adv. 4 (2) (2018) 4223, doi:10.1126/sciadv.aao4223.
[16] N.M. Litchinitser, J. Sun, Optical meta-atoms: going nonlinear, Science 350 (6264) (2015) 1033–1034, doi:10.1126/science.aad7212.
[17] N.I. Zheludev, E. Plum, Reconfigurable nanomechanical photonic metamaterials, Nat. Nanotechnol. 11 (1) (2016) 16–22, doi:10.1038/nnano.2015.302.
[18] J.B. Pendry, Negative refraction makes a perfect lens, Phys. Rev. Lett. 85 (18) (2000) 3966, doi:10.1103/PhysRevLett.85.3966.
[19] N.I. Landy, S. Sajuyigbe, J.J. Mock, D.R. Smith, W.J. Padilla, Perfect metamaterial absorber., Phys. Rev. Lett. 100 (20) (2008) 207402, doi:10.1103/PhysRevLett.100.207402.
[20] W. Cai, U.K. Chettiar, A.V. Kildishev, V.M. Shalaev, Optical cloaking with metamaterials, Nat. Photonics 1 (2007) 224–227, doi:10.1038/nphoton.2007.28.
[21] H. Fang, S.A. Chu, Y. Xia, K.W. Wang, Programmable self-locking origami mechanical metamaterials., Adv. Mater. 30 (15) (2018) e1706311, doi:10.1002/adma.201706311.
[22] D.Z. Rocklin, S. Zhou, K. Sun, X. Mao, Transformable topological mechanical metamaterials., Nat. Commun. 8 (2017) 14201, doi:10.1038/ncomms14201.
[23] T. Frenzel, M. Kadic, M. Wegener, Three-dimensional mechanical metamaterials with a twist, Science 358 (6366) (2017) 1072–1074, doi:10.1126/science.aao4640.
[24] C. Coulais, D. Sounas, A. Alu, Static non-reciprocity in mechanical metamaterials, Nature 542 (7642) (2017) 461, doi:10.1038/nature21044.
[25] J.B. Berger, H.N.G. Wadley, R.M. McMeeking, Mechanical metamaterials at the theoretical limit of isotropic elastic stiffness, Nature 543 (7646) (2017) 533, doi:10.1038/nature21075.
[26] Q. Wang, J.A. Jackson, Q. Ge, J.B. Hopkins, C.M. Spadaccini, N.X. Fang, Lightweight mechanical metamaterials with tunable negative thermal expansion, Phys. Rev. Lett. 117 (17) (2016) 175901, doi:10.1103/PhysRevLett.117.175901.
[27] C. Huang, L. Chen, Negative Poisson's ratio in modern functional materials, Adv. Mater. 28 (37) (2016) 8079–8096, doi:10.1002/adma.201601363.
[28] Y. Du, J. Maassen, W. Wu, Z. Luo, X. Xu, P.D. Ye, Auxetic Black Phosphorus: A 2D material with negative Poisson's ratio, Nano Lett. 16 (10) (2016) 6701–6708, doi:10.1021/acs.nanolett.6b03607.
[29] H. Zhu, T. Fan, Q. Peng, D. Zhang, Giant thermal expansion in 2D and 3D cellular materials, Adv. Mater. 30 (18) (2018) 1705048, doi:10.1002/adma.201705048.
[30] A. Rafsanjani, A. Akbarzadeh, D. Pasini, Snapping mechanical metamaterials under tension., Adv. Mater. 27 (39) (2015) 5931–5935, doi:10.1002/adma.201502809.
[31] S. Shan, S.H. Kang, J.R. Raney, P. Wang, L. Fang, F. Candido, J.A. Lewis, K. Bertoldi, Multistable architected materials for trapping elastic strain energy, Adv. Mater. 27 (29) (2015) 4296–4301, doi:10.1002/adma.201501708.
[32] T. Buckmann, M. Thiel, M. Kadic, R. Schittny, M. Wegener, An elasto-mechanical unfeelability cloak made of pentamode metamaterials, Nat. Commun. 5 (2014) 4130, doi:10.1038/ncomms5130.
[33] S.A. Cummer, J. Christensen, A. Alù, Controlling sound with acoustic metamaterials, Nat. Rev. Mater. 1 (2016) 16001, doi:10.1038/natrevmats.2016.1.
[34] Zheng G., Y. Qiu, M.J. Griffin, An analytic model of the in-line and cross-axis apparent mass of the seated human body exposed to vertical vibration with

and without a backrest, J. Sound Vib. 330 (26) (2011) 6509–6525, doi:10.1016/j.jsv.2011.06.026.
[35] J. Zhou, K. Wang, D. Xu, H. Ouyang, Y. Fu, Vibration isolation in neonatal transport by using a quasi-zero-stiffness isolator, J. Vib. Control 24 (15) (2017) 3278–3291, doi:10.1177/1077546317703866.
[36] L. Blaxter, M. Yeo, D. McNally, J. Crowe, C. Henry, S. Hill, N. Mansfield, A Leslie, D Sharkey, Neonatal head and torso vibration exposure during inter-hospital transfer, Proc. Inst. Mech. Eng. Part H 231 (2) (2017) 99–113, doi:10.1177/0954411916680235.
[37] R Savickas, L. Gailiūnienė, G. Krutulytė, V. Šiaučiūnaitė, M. Venslauskas, The effect of low frequency 2-10 Hz vibrations on blood circulation in lower extremities, J. Vibroengineering 19 (6) (2017) 4694–4701, doi:10.21595/jve.2017.18381.
[38] X. Wang, H. Liu, Y. Chen, P. Gao, Beneficial stiffness design of a high-static-low-dynamic-stiffness vibration isolator based on static and dynamic analysis, Int. J. Mech. Sci. 142-143 (2018) 235–244, doi:10.1016/j.ijmecsci.2018.04.053.
[39] S. Ishida, H. Uchida, H. Shimosaka, I. Hagiwara, Design and numerical analysis of vibration isolators with Quasi-zero-stiffness characteristics using bistable foldable structures, J. Vib. Acoust. 139 (3) (2017) 031015, doi:10.1115/1.4036096.
[40] Y. Wang, X. Jing, Design of a novel quasi-zero-stiffness based sensor system for measurement of absolute vibration motion, in: 2015 10th Asian Control Conference (ASCC), IEEE: Kota Kinabalu, Malaysia, 2015, pp. 1–6, doi:10.1109/ASCC.2015.7244435.
[41] J. Zhou, X. Wang, Y. Mei, Characteristic analysis of a quasi-zero-stiffness vibration isolator, IOP Conf. Ser. 397 (2018) 012045, doi:10.1088/1757-899X/397/1/012045.
[42] K. Inamoto, S. Ishida, Improved feasible load range and its effect on the frequency response of origami-inspired vibration isolators with quasi-zero-stiffness characteristics, ASME 2018 Int. Design Eng. Tech. Conf. Comput. Inf. Eng. Conf. Vol. 8: 30th Conf. Mechanical Vibration and Noise, ASME, Quebec, Canada, 2018, doi:10.1115/DETC2018-85765.
[43] S. Ishida, K. Suzuki, H. Shimosaka, design and experimental analysis of origami inspired vibration isolator with quasi zero stiffness characteristic, J. Vib. Acoust. 139 (5) (2017) 051004, doi:10.1115/1.4036465.
[44] Y. Zheng, X. Zhang, Y. Luo, B. Yan, C. Ma, Design and experiment of a high-static–low-dynamic stiffness isolator using a negative stiffness magnetic spring, J. Sound Vib. 360 (2016) 31–52, doi:10.1016/j.jsv.2015.09.019.
[45] M.A. Beijen, M.F. Heertjes, H. Butler, M. Steinbuch, Disturbance feedforward control for active vibration isolation systems with internal isolator dynamics, J. Sound Vib. 436 (2018) 220–235, doi:10.1016/j.jsv.2018.09.010.
[46] J. Ding, X. Luo, X. Chen, O. Bai, B. Han, Design of active controller for low-frequency vibration isolation considering noise levels of bandwidth-extended absolute velocity sensors, IEEE/ASME Trans. Mechatronics 23 (4) (2018) 1832–1842, doi:10.1109/TMECH.2018.2843558.
[47] M. Friedman, Visual control of head movements during avian locomotion, Nature 255 (1975) 67–69, doi:10.1038/255067a0.